Inorg. Chem. **2005**, *44*, 3799–3809

Substituent-Directed Structural and Physicochemical Controls of Diruthenium Catecholate Complexes with Ligand-Unsupported Ru–Ru Bonds

Ho-Chol Chang,[†,‡,§] Katsunori Mochizuki,[†] and Susumu Kitagawa*[,†]

Department of Synthetic Chemistry and Biological Chemistry, Graduate School of Engineering, Kyoto University, Katsura, Nishikyo-ku, Kyoto 615-8510, Japan, and PRESTO, Japan Science and Technology Agency, 4-1-8 Honcho, Kawaguchi, Saitama 332-0012, Japan

Received December 13, 2004

A family of diruthenium complexes with ligand-unsupported Ru–Ru bonds has been systematically synthesized, and their crystal structures and physical properties have been examined. A simple, useful reaction between $Ru_2(OAc)_4Cl$ (OAc^- = acetate) and catechol derivatives in the presence of bases afforded a variety of diruthenium complexes, generally formulated as $[Na_n\{Ru_2(R_4Cat)_4\}]$ ($n = 2$ or 3; $R_4 = -F_4$, $-Cl_4$, $-Br_4$, $-H_4$, –3,5-di-*t*-Bu, and –3,6-di-*t*-Bu; Cat^{2-} = catecholate). The most characteristic feature of the complexes is the formation of short ligand-unsupported Ru–Ru bonds (2.140–2.273 Å). These comprehensive studies were carried out to evaluate the effects of the oxidation states and the substituents governing the molecular structures and physicochemical properties. The Ru–Ru bond distances, rotational conformations, and bending structures of the complexes were successfully varied. The results presented in this manuscript clearly demonstrate that the complexes with ligand-unsupported Ru–Ru bonds can sensitively respond to redox reactions and ligand substituents on the basis of the greater degree of freedom in their molecular structures.

1. Introduction

Complexes with direct metal−metal (M−M) bonds have received considerable attention in studies on the influence of electron configurations and molecular structures for multiple bond systems. Studies of multiple M−M bonds between transition metals within discrete complexes offer fundamental insight into the nature of bonding interactions between two or more metal atoms.[1]

Development of the synthetic methods of M−M-bonded complexes is of great importance for an in-depth understanding of M−M bonding interactions, electronic configurations, and their reactivity. Among the M−M-bonded compounds, "dinuclear complexes" have been studied more extensively in connection with a rational synthesis and characterization of the multiple bond systems. In most previous work, two metal ions were connected by bridging ligands such as carboxylates (−OOR) to form a dinuclear complex, $[M_2(OOR)_4]^{n+}$, with a so-called paddle-wheel type structure.[2] The bridging ability of these ligands strongly promotes the formation of the M−M bonds, supported by the orbital interactions between the well-oriented metal- and ligand-based orbitals. As a result, the bridging ligands advantageously restrict structures of the complexes by minimizing the structural deviation or deformation of the dimetallic unit caused not only by chemical stimuli such as redox reactions, axial coordination, and the ligand substituents but also by physical stimuli, for example, temperature. The continuing study has provided a diversity of complexes and has led to attractive properties such as inorganic liquid crystals,[3a,b] one-dimensional polymers,[3c,d] supramolecular assemblies,[3e] antitumor reagents,[3f] and conductive[3g] and magnetic materials.[3h,i]

In contrast to the paddle-wheel complexes, some complexes have been known to possess *ligand-unsupported* M−M bonds that have no support from any bridging ligands.[4] The liberation from the bridging structure in part realizes different potentials for the M−M-bonded systems.

* Author to whom correspondence should be addressed. E-mail: kitagawa@sbchem.kyoto-u.ac.jp. Tel: +81-75-383-2733. Fax: +81-75-383-2732.
† Kyoto University.
‡ PRESTO.
§ E-mail: chang@sbchem.kyoto-u.ac.jp.

(1) Cotton, F. A.; Walton, R. A. *Multiple Bonds Between Metal Atoms*, 2nd ed.; Oxford University Press: Oxford, England, 1993.

(2) (a) Boyar, E. B.; Robinson, S. D. *Coord. Chem. Rev.* **1983**, *50*, 109. (b) Aquino, M. A. S. *Coord. Chem. Rev.* **1998**, *170*, 141.

10.1021/ic048251m CCC: $30.25
Published on Web 04/28/2005

Chart 1. Catecholate Derivatives Used in This Study

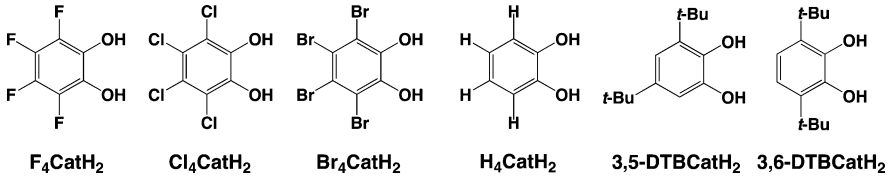

One fascinating subject has been the investigation of the inherent strength of the δ bond, which leads to the formation of a quadruple M−M bond.[5] However, the variety of ligand-unsupported M−M bonds is quite limited compared with those of the ligand-supported family, although it is an important subject to clarify and control the nature of the M−M bond and its functions.

In 1998, we developed a reaction for synthesizing ruthenium complexes with ligand-unsupported Ru−Ru bonds.[6] The reaction between $Ru_2(OAc)_4Cl$ (OAc^- = acetate) with tetrachlorocatecholate (Cl_4CatH_2) afforded complexes $[Na(THF)_5][\{Na(THF)(H_2O)_{1.5}\}_2\{Ru_2(Cl_4Cat)_4(THF)\}]$ (**2**$_s$) and $[\{Na(THF)(H_2O)\}_2\{Ru_2(Cl_4Cat)_4(THF)_2\}]$ (**2′**$_s$), as a result of ligand substitution of four OAc^- ligands by the four Cl_4Cat^{2-}. The structural characterization shows that these complexes possess ligand-unsupported Ru−Ru bonds with short Ru−Ru bonds, 2.273(1) (**2**$_s$) and 2.2233(6) Å (**2′**$_s$). The transformation of ligand-supported Ru−Ru bonds to ligand-unsupported Ru−Ru bonds has great potential for developing new synthetic entries into dimetallic complexes with ligand-unsupported M−M bonds. Our previous X-ray structural determination provided good candidates and a starting point from which to launch the systematic examination of ligand-unsupported M−M-bonded systems stabilized by catecholates. To better understand, and even control, the ligand-unsupported Ru−Ru bond, it is very important to obtain a deeper insight into both the molecular structures and also the electronic structures of the ligand-unsupported M−M bond in a controlled manner. In addition, the internal freedoms in molecular structures and electronic structures, which are derived from the ligand-unsupported M−M bonds, should be carefully examined in connection with the response against chemical and physical stimuli. The goals of the present research were 2-fold. First, the molecular structures of the complexes were crystallographically investigated in connection with the substituent groups of the catecholates. Six different substituent groups were introduced to catecholate ring, as drawn in Chart 1, where each ligand differs in the type of substituents on the catecholate ring and the position of the substituents. Given the abundance of substituent tuning in paddle-wheel type dinuclear complexes,[7] it is surprising that there are no existing examples for the dinuclear complexes with ligand-unsupported M−M bonds. By using these ligands, we examined the electronic and steric effects of the substituents both in the solid state and in solution. Second, it was important to elucidate the electronic configuration of the target complexes. The chemical oxidations were performed, and the structures and properties of different redox isomers were compared. We will describe each result in the following sections and discuss the important parameters governing both the molecular structures and electronic structures of dinuclear complexes to give a new route for developing the usefulness of the M−M-bonded system as a molecular building block.

2. Experimental Section

2.1. Materials and Methods. Tetrakis(acetato)diruthenium chloride ($Ru_2(OAc)_4Cl$),[8] tetrafluorocatechol (F_4CatH_2),[9] 3,6-di-*tert*-butylcatechol (3,6-DTBCatH_2),[10] $[Na_3\{Ru_2(Cl_4Cat)_4(THF)\}]\cdot 3THF\cdot 3H_2O$ (**2**),[6] and $[Na_2\{Ru_2(Cl_4Cat)_4(THF)_2\}]\cdot 2H_2O$ (**2′**)[6] were synthesized by the literature methods. The other chemicals were purchased from Aldrich Co. (silver trifluoroacetate ($AgOCOCF_3$)), Lancaster (tetrabromocatechol (Br_4CatH_2)), Tokyo Chemical Industry Co., Ltd. (catechol (H_4CatH_2), 3,5-di-*tert*-butylcatechol (3,5-DTBCatH_2), and tetra-*n*-butylammonium hexafluorophosphate (*n*-Bu_4NPF_6)), and Nacalai Tesque, Inc. (sodium hydroxide (NaOH)). All of the solvents (tetrahydrofuran (THF), *n*-hexane (hexane), 1,2-dimethoxyethane (DME), *N*,*N*-dimethylformamide (DMF), acetone, and benzene) were distilled by standard methods under a dinitrogen atmosphere. All synthetic operations were performed under a dinitrogen atmosphere.

2.2. Abbreviations for the Complexes. The complexes with the $[Ru_2]^{6+}$ core are distinguished by adding a prime (′) after the number. Because the single crystals and the polycrystalline samples of **2**, **3**, **2′**, **3′**, and **6′** have different compositions, these are distinguished by adding "s" in a subscript form after each

(3) (a) Rusjan, M.; Donnio, B.; Guillon, D.; Cukiernik, F. D. *Chem. Mater.* **2002**, *14* 1564. (b) Chisholm, M. H. *Acc. Chem. Res.* **2000**, *33*, 53. (c) Cotton, F. A.; Kim, Y.; Ren, T. *Inorg. Chem.* **1992**, *31*, 2723. (d) Wesemann, J. L.; Chisholm, M. H. *Inorg. Chem.* **1997**, *36*, 3258. (e) Cotton, F. A.; Lin, C.; Murillo, C. A. *Acc. Chem. Res.* **2001**, *34*, 759. (f) Chifotides, H. T.; Koshlap, K. M.; Perez, L. M.; Dunbar, K. R. *J. Am. Chem. Soc.* **2003**, *125*, 10714. (g) Mitsumi, M.; Murase, T.; Kishida, H.; Yoshinari, T.; Ozawa, Y.; Toriumi, K.; Sonoyama, T.; Kitagawa, H.; Mitani, T. *J. Am. Chem. Soc.* **2001**, *123*, 11179−11192. (h) William, Y. L.; Shum, W.; Miller, J. S. *J. Am. Chem. Soc.* **2002**, *124*, 9336. (i) Jimenez-Aparicio, R.; Urbanos, F. A.; Arrieta, J. M. *Inorg. Chem.* **2001**, *40*, 613.

(4) (a) Cotton, F. A.; Eglin, J. L. *Inorg. Chim. Acta* **1992**, *198*−*200*, 13. (b) Collman, J. P.; Arnold, H. J. *Acc. Chem. Res.* **1993**, *26*, 586. (c) Prater, M. E.; Pence, L. E.; Clérac, R.; Finniss, G. M.; Campana, C.; Auban-Senzier, P.; Jérome, D.; Canadell, E.; Dunbar, K. R. *J. Am. Chem. Soc.* **1999**, *121*, 8005. (d) Chern, S.-S.; Liaw, M.-C.; Peng, S.-M. *J. Chem. Soc., Chem. Commun.* **1993**, 359.

(5) (a) Cotton, F. A.; Nocera, D. G. *Acc. Chem. Res.* **2000**, *33*, 483. (b) Collman, J. P.; Garner, J. M.; Hembre, R. T.; Ha, Y. *J. Am. Chem. Soc.* **1992**, *114*, 1292. (c) Hopkins, M. D.; Gray, H. B. *Polyhedron* **1987**, *6*, 705.

(6) Kondo, M.; Hamatani, M.; Kitagawa, S. *J. Am. Chem. Soc.* **1998**, *120*, 455.

(7) (a) Kadish, K. M.; Wang, L.-L.; Thuriere, A.; Caemelbecke, E. V.; Bear, J. L. *Inorg. Chem.* **2003**, *42*, 834. (b) Ren, T. *Coord. Chem. Rev.* **1998**, *175*, 43. (c) Lin, C.; Ren, T.; Valente, E. J.; Zubkowski, J. D. *J. Chem. Soc., Dalton Trans.* **1998**, 571.

(8) (a) Stephenson, T. A.; Wilkinson, G. *J. Inorg. Nucl. Chem.* **1966**, *28*, 2285. (b) Mitchell, R. W.; Spencer, A.; Wilkinson, G. *J. Chem. Soc., Dalton Trans.* **1973**, 846.

(9) (a) Burdon, B. J.; Damodaran, V. A.; Tatlow, J. C. *J. Chem. Soc.* **1964**, 763. (b) Macdonald, C.; Tomlinson, A. J.; Willis, C. J. *Can. J. Chem.* **1971**, *49*, 2578.

(10) Belostotskaya, I. S.; Komissarova, N. L.; Dzhuaryan, E. V.; Ershov, V. V. *Izv. Nauk. Khim. SSSR* **1972**, *7*, 1594.

abbreviation number for single crystalline samples. The samples with "s" were used for the structural analyses, while those without "s" were used for elemental analysis, magnetic measurements, and spectroscopic and electrochemical studies. Only the abbreviation numbers are used for **1**, **4**, **1′**, and **4′** without the use of "s".

2.3. Procedure for Preparation. 2.3.1. General Procedure for Preparation of 1, 3, 4, 5′, and 6′. A THF suspension containing $Ru_2(OAc)_4Cl$ and 4 equiv of R_4CatH_2 ($R_4 = -F_4$ (**1**), $-Br_4$ (**3**), $-H_4$ (**4**), −3,5-DTB (**5′**), and −3,6-DTB (**6′**)) and 8 equiv of NaOH was stirred for 1 day at room temperature. The violet or reddish-purple suspensions were dried under vacuum and then extracted with THF (**1**, **3**, **5′**, and **6′**) or DMF (**4**). The crystalline products were obtained by slow diffusion of hexane (**1**, **3**, and **6′**), benzene (**4**), or DME (**5′**) onto the solutions.

$[Na_3\{Ru_2(F_4Cat)_4\}]\cdot 2THF\cdot 2H_2O$ (1). Yield: 72%. Anal. Calcd for $C_{32}H_{20}F_{16}Na_3O_{12}Ru_2$ (**1**): C, 32.81; H, 1.72. Found: C, 32.91; H, 1.94. Paramagnetic data: $\mu_{eff} = 1.28$ (2 K) and 1.67 μ_B (300 K). UV−vis−NIR (λ_{max}/nm (ϵ/$M^{-1}\cdot cm^{-1}$) in THF): 270 (sh), 475 (sh), 633 (6700), 850 (sh).

$[Na_3\{Ru_2(Br_4Cat)_4\}]\cdot 4THF\cdot 2H_2O$ (3). Yield: 86%. Anal. Calcd for $C_{40}H_{36}Br_{16}Na_3O_{14}Ru_2$ (**3**): C, 20.98; H, 1.58. Found: C, 20.82; H, 1.50. A single crystal, $[Na\{Na(acetone)(H_2O)\}_2\{Ru_2(Br_4Cat)_4\}]\cdot$ 2acetone (**3_s**), was obtained by slow diffusion of hexane onto the acetone solution of **3**. Paramagnetic data (**3**): $\mu_{eff} = 0.99$ (2 K) and 1.63 μ_B (300 K). UV−vis−NIR (λ_{max}/nm (ϵ/$M^{-1}\cdot cm^{-1}$) in THF): 306 (23 500), 552 (7970), 850 (sh).

$[Na\{Na(DMF)\}_2\{Ru_2(H_4Cat)_4\}]$ (4). Yield: 72%. Anal. Calcd for $C_{30}H_{30}N_2Na_3O_{10}Ru_2$ (**4**): C, 42.41; H, 3.56; N, 3.30. Found: C, 41.95; H, 3.36; N, 3.24. Paramagnetic data: $\mu_{eff} = 1.30$ (2 K) and 1.66 μ_B (300 K). UV−vis−NIR (λ_{max}/nm (ϵ/$M^{-1}\cdot cm^{-1}$) in DMF): 302 (26 100), 346 (11 300), 522 (10 800), 700 (sh).

$[\{Na(DME)_2\}_2\{Ru_2(3,5\text{-}DTBCat)_4\}]$ (5′). Yield: 53%. Anal. Calcd for $C_{72}H_{120}Na_2O_{16}Ru_2$ (**5′**): C, 58.04; H, 8.12. Found: C, 58.03; H, 7.99. The complex is diamagnetic. UV−vis−NIR (λ_{max}/nm (ϵ/$M^{-1}\cdot cm^{-1}$) in THF): 299 (29 000), 420 (sh), 518 (15 200), 700 (sh).

$[Na_2\{Ru_2(3,6\text{-}DTBCat)_4\}]$ (6′). A single crystal, $[\{Na(THF)_2\}_2Ru_2$-(3,6-DTBCat)$_4$] (**$6'_s$**), easily loses the cocrystallized solvents under vacuum. The polycrystalline sample formulated as $[Na_2\{Ru_2(3,6$-DTBCat)$_4\}]$ was obtained by drying the single crystals under vacuum. Yield: 62%. Anal. Calcd for $C_{56}H_{80}Na_2O_8Ru_2$ (**6′**): C, 59.56; H, 7.14. Found: C, 58.99; H, 7.69. The complex is diamagnetic. UV−vis−NIR (λ_{max}/nm (ϵ/$M^{-1}\cdot cm^{-1}$) in THF): 293 (17 800), 514 (12 700), 700 (sh).

2.3.2. General Procedure for Preparation of 1′, 3′, and 4′. A THF or DMF solution of single-crystalline samples of **1**, **3**, and **4** was combined with a solution of $AgOCOCF_3$ in the same solvent with stirring. The resultant suspensions were stirred for 1 day, giving violet suspensions. The suspensions were dried and then extracted with THF. Slow diffusion of hexane onto the solutions gave single-crystal or powder products.

$[Na_2\{Ru_2(F_4Cat)_4\}]\cdot 3THF$ (1′). Yield: 40%. Anal. Calcd for $C_{36}H_{24}F_{16}Na_2O_{11}Ru_2$ (**1′**): C, 36.50; H, 2.04. Found: C, 36.18; H, 2.27. The complex is diamagnetic. UV−vis−NIR (λ_{max}/nm (ϵ/$M^{-1}\cdot cm^{-1}$) in THF): 267 (sh), 572 (5510).

$[Na_2\{Ru_2(Br_4Cat)_4(THF)_2\}]\cdot 3THF$ (3′). The single crystal, $[\{Na(THF)_2\}_2\{Ru_2(Br_4Cat)_4(THF)_2\}]$ (**$3'_s$**), easily loses the co-crystallized solvent under vacuum. The polycrystalline sample formulated as $[Na_2\{Ru_2(Br_4Cat)_4(THF)_2\}]\cdot 3THF$ was obtained by drying the single crystals under vacuum. Yield: 86%. Anal. Calcd for $C_{44}H_{40}Br_{16}Na_2O_{13}Ru_2$ (**3′**): C, 22.94; H, 1.75. Found: C, 23.22; H, 1.85. The complex is diamagnetic. UV−vis−NIR (λ_{max}/nm (ϵ/$M^{-1}\cdot cm^{-1}$) in THF): 295 (24 900), 557 (8500), 703 (9600), 810 (sh).

$[Na_2\{Ru_2(H_4Cat)_4\}]\cdot 2THF$ (4′). Yield: 75%. Anal. Calcd for $C_{32}H_{32}Na_2O_{10}Ru_2$ (**4′**): C, 46.60; H, 3.91. Found: C, 46.62; H, 4.09. The complex is diamagnetic. UV−vis−NIR (λ_{max}/nm (ϵ/$M^{-1}\cdot cm^{-1}$) in THF): 304 (24 500), 557 (10 900).

2.4. Physical Measurements. Absorption spectra were recorded on a Hitachi U-3500 spectrophotometer over the range 185−3200 nm at 296 K. Electrochemical measurements were carried out with a BAS model 650A electrochemical analyzer. A standard three-electrode system was used with a glassy carbon working electrode, platinum-wire counter electrode, and $Ag/Ag^+/CH_3CN$ electrode as reference (all of the potentials in the figures and table are given as volts vs ferrocene/ferrocenium (Fc/Fc^+)). Magnetic susceptibilities were recorded over the temperature range 2.0−300 K at 1 T with a superconducting quantum interference device (SQUID) susceptometer (Quantum Design, San Diego, CA) interfaced with a HP Vectra computer system. All of the values were corrected for diamagnetism using Pascal's constants.[12] EPR spectra were recorded with a JEOL RE-3X spectrometer operating at 9.0−9.2 GHz at 77 K. The resonance frequency was measured on an Anritsu MF76A microwave frequency counter. The magnetic field was calibrated with an Echo Electronics EMF-2000AX NMR field meter.

2.5. Crystallographic Data Collection and Refinement of Structures. All crystallographic measurements were performed on a Rigaku mercury diffractometer with a CCD two-dimensional detector with Mo Kα radiation employing a graphite monochromator. The sizes of the unit cells were calculated from the reflections collected on the setting angles of seven frames by changing ω by 0.5° for each frame. Two or three different χ settings were used, and ω was changed by 0.5°/frame. Intensity data were collected in 480−1080 frames with an ω scan width of 0.5°. Empirical absorption correction using the program REQABA[13] was performed for **4**, while numerical absorption corrections were performed for all of the others. All of the crystallographic data are summarized in Table 1. The structures were solved by direct methods for **3_s** and **$3'_s$**[14a] or the Patterson method[14b] for the others and expanded using Fourier techniques.[15] The final cycles of the full-matrix least-squares refinements were based on the observed reflections ($I > 3\sigma(I)$ for **$3'_s$**, **5′**, and **$6'_s$**, and $I > 4\sigma(I)$ for the others). All of the calculations were performed using the teXsan crystallographic software package from Molecular Structure Corp.[16] For **4**, one of the two DMF molecules (C(28)−C(30), N(2), O(10), and H(24)−H(30)) was refined under condition of rigidity. There are highly disordered −*t*-Bu groups, C(26)−C(28), in **5′**. The C(8)−C(10) and C(26)−C(28) in **$6'_s$** are disordered. The positions

(11) Chang, H.-C.; Mochizuki, K.; Kitagawa, S. *Inorg. Chem.* **2005**, *44*, 3810−3817.
(12) Boudreaux, E. A.; Mulay, L. N. *Theory and Applications of Molecular Paramagnetism*; John Wiley and Sons: New York, 1976; pp 491−495.
(13) REQABA: Jacobson, R. A. *REQABA Empirical Absorption Correction*, version 1.1−03101998; Molecular Structure Corp.: The Woodlands, TX, 1996−1998.
(14) (a) SIR97: Altomare, A.; Burla, M. C.; Camalli, M.; Cascarano, G. L.; Giacovazzo, C.; Guagliardi, A.; Moliterni, A. G. G.; Polidori, G.; Spagna, R. *J. Appl. Crystallogr.* **1999**, *32*, 115−119. (b) PATTY: Beurskens, P. T.; Admiraal, G.; Beurskens, G.; Bosman, W. P.; de Gelder, R.; Israel, R.; Smits, J. M. M. *The DIRDIF program system*; Technical Report of the Crystallography Laboratory, University of Nijmegen: Nijmegen, The Netherlands, 1994.
(15) DIRDIF94: Beurskens, P. T.; Admiraal, G.; Beurskens, G.; Bosman, W. P.; de Gelder, R.; Israel, R.; Smits, J. M. M. *The DIRDIF program system*; Technical Report of the Crystallography Laboratory, University of Nijmegen: Nijmegen, The Netherlands, 1994.
(16) *teXsan: Crystal Structure Analysis Package*; Molecular Structure Corp.: The Woodlands, TX, 1985, 1992.

Table 1. Crystallographic Data for $[Na_n\{Ru_2(R_4Cat)_4\}]$ ($n = 3$, $R_4 = -Br_4$ and $-H_4$; $n = 2$, $R_4 = -Br_4$, $-3,5$-DTB, and $-3,6$-DTB)

param	$[Na\{Na(acetone)(H_2O)\}_2\{Ru_2(Br_4Cat)_4\}]\cdot 2$acetone (**3s**)	$[Na\{Na(DMF)\}_2\{Ru_2(H_4Cat)_4\}]$ (**4**)	$[\{Na(THF)_2\}_2\{Ru_2(Br_4Cat)_4(THF)_2\}]$ (**3′s**)	$[\{Na(DME)_2\}_2\{Ru_2(3,5\text{-DTBCat})_4\}]$ (**5′**)	$[\{Na(THF)_2\}_2\{Ru_2(3,6\text{-DTBCat})_4\}]$ (**6′s**)
formula	$C_{36}H_{28}Br_{16}Na_3O_{14}Ru_2$	$C_{30}H_{30}N_2Na_3O_{10}Ru_2$	$C_{48}H_{48}Br_{16}Na_2O_{14}Ru_2$	$C_{72}H_{120}Na_2O_{16}Ru_2$	$C_{72}H_{112}Na_2O_{12}Ru_2$
fw	2234.18	849.68	2375.48	1489.85	1417.79
cryst system	monoclinic	triclinic	triclinic	monoclinic	trigonal
space group	$P2_1/c$	$P\bar{1}$	$P\bar{1}$	$P2_1/c$	$P3_112$
color of cryst	violet	red	violet	purple	purple
a, Å	12.724(2)	11.568(3)	13.287(2)	11.073(2)	13.8142(5)
b, Å	27.929(3)	12.233(4)	14.054(2)	16.211(2)	
c, Å	15.907(2)	13.014(4)	18.642(2)	22.136(3)	33.628(2)
α, deg		96.90(1)	90.994(6)		
β, deg	97.630(3)	113.13(2)	95.842(4)	100.146(3)	
γ, deg		101.25(2)	105.648(6)		
V, Å^3	5602.7(1)	1621.1(9)	3330.9(7)	3911.5(9)	5557.6(4)
temp, K	223	296	223	223	223
Z	4	2	2	2	3
D_{calcd}, g·cm^{-3}	2.648	1.741	2.368	1.265	1.271
no. of reflcns	7808[a]	5026[a]	8087[b]	5649[a]	2254
no. of params	640	399	739	415	322
GOF	1.15	1.54	1.22	1.27	1.22
R_{int}	0.042	0.027	0.033	0.028	0.051
R, R_w[c]	0.054, 0.094	0.058, 0.095	0.066, 0.086	0.040, 0.055	0.093, 0.133

[a] $I > 4.0\sigma(I)$. [b] $I > 3.0\sigma(I)$. [c] $R = \Sigma||F_o| - |F_c||/\Sigma|F_o|$ and $R_w = [\Sigma w(|F_o| - |F_c|)^2/\Sigma w|F_o|^2]^{1/2}$.

Scheme 1. Synthetic Scheme for Diruthenium Complexes with Ligand-Unsupported Ru−Ru Bonds

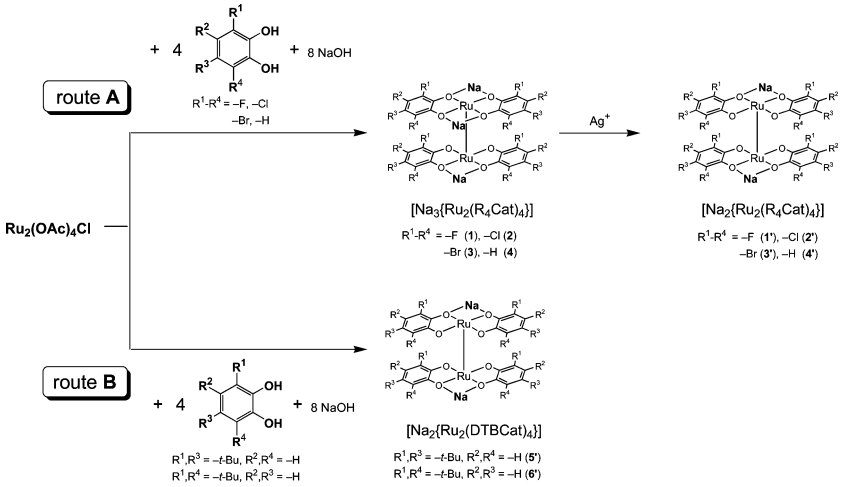

of two independent THF molecules (O(5)−O(6), C(29)−C(36), and H(41)−H(56)) in **6′s** were fixed during the refinements.

3. Results and Discussion

3.1. Synthesis of $[Na_3\{Ru_2(R_4Cat)_4\}]$ with Ligand-Unsupported Ru−Ru Bonds. All synthetic manipulations were performed by standard inert-atmosphere techniques, because solutions of the complexes are extremely sensitive to air.[6] A reaction of $Ru_2(OAc)_4Cl$ with catecholate derivatives R_4CatH_2 ($R_4 = -F_4$, $-Cl_4$, $-Br_4$, and $-H_4$) was carried out in the presence of NaOH in THF according to route A in Scheme 1. An original brown suspension gradually changed to a deep violet solution (**1**−**3**) or reddish-purple suspension (**4**), affording deep colored polycrystalline solids or single crystals on subsequent recrystallization. The elemental analyses and single-crystal structural characterization support the contention that the solid products are generally formulated as $[Na_3\{Ru_2(R_4Cat)_4\}]$ (eq 1), possessing three Na^+ cations/dimeric unit. Each complex was commonly cocrystallized with solvent molecules such as THF, H_2O, and DMF, and all of the complexes were fairly soluble in common organic solvents such as THF and CH_2Cl_2 except for **4**, which is soluble only in DMF and DMSO.

$$Ru_2(OAc)_4Cl + 4R_4CatH_2 + 8NaOH \rightarrow [Na_3\{Ru_2(R_4Cat)_4\}]\ (\mathbf{1}-\mathbf{4}) + 4NaOAc + NaCl + 8H_2O \quad (1)$$

3.2. Molecular Structures of $[Na_3\{Ru_2(R_4Cat)_4\}]$ with Ligand-Unsupported Ru−Ru Bonds. The crystallographic data and structural parameters for the complexes are listed in Tables 1 and 2, respectively. As shown in Figure 1, the structural analyses provide useful information about the unique Ru−Ru bonded structures of the dinuclear complexes. Two cofacial [Ru(dioxolene)$_2$] units are combined together by the Ru−Ru bond without bridging ligands, which have been widely used in the paddle-wheel type diruthenium complexes.[1,17] Each Ru atom has either a six-coordinated

(17) (a) Bear, J. L.; Li, Y.; Han, B.; Kadish, K. M. *Inorg. Chem.* **1996**, *35*, 1395. (b) Bear, J. L.; Li, Y.; Han, B.; Caemelbecke, E. V.; Kadish, K. M. *Inorg. Chem.* **1997**, *36*, 5449. (c) Miyasaka, H.; Kachi-Terajima, C.; Ishii, T.; Yamashita, M. *J. Chem. Soc., Dalton Trans.* **2001**, 1929.

Table 2. Structural Parameters of $[Na_n\{Ru_2(R_4Cat)_4\}]$ ($n = 3$, $R_4 = -Cl_4$, $-Br_4$, and $-H_4$; $n = 2$, $R_4 = -Cl_4$, $-Br_4$, $-3,5$-DTB, and $-3,6$-DTB)

Complex	R_4	Ru−Ru/Å	Ru−O_{Cat} (av)/Å	C−O_{Cat} (av)/Å	deviatn *d*/Å	Ru−Ru−O_{Cat} (av)/deg	twist angle *θ*/deg	ax ligands	Ru−O_{THF}/Å	assembled struct
$\mathbf{2_s}$[a,b]	$-Cl_4$	2.273(1)	2.019	1.33	0.271(3)	97.7	1.6	1	2.434(7)	polymeric
					0.363(3)	100.4				
$\mathbf{3_s}$[b]	$-Br_4$	2.249(1)	2.001	1.34	0.359(4)	100.3	19.5	0		polymeric
					0.345(4)	99.9				
4[c] (i)	$-H_4$	2.2540(8)	2.005	1.353	0.373(3)	100.7	0.6	0		polymeric
4[c] (ii)	$-H_4$	2.246(1)	2.005	1.347	0.388(3)	101.2	2.1	0		
$\mathbf{2'_s}$[a]	$-Cl_4$	2.2233(6)	1.982	1.353	0.325(1)	99.51	3.6	2	2.647(3)	polymeric
$\mathbf{3'_s}$[b]	$-Br_4$	2.196(1)	1.982	1.36	0.282(4)	98.2	22.4	2	2.513(9)	discrete
					0.291(4)	98.5			2.498(9)	
5′	−3,5-DTB	2.1698(6)	1.969	1.363	0.486(1)	104.26	1.58	0		discrete
$\mathbf{6'_s}$	−3,6-DTB	2.140(2)	1.97	1.37	0.509(5)	105.2	50.8	0		discrete

[a] Reference 6. [b] There are one crystallographically independent dimer unit and two independent Ru atoms. [c] There are two crystallographically independent dimer units with one independent Ru atom each.

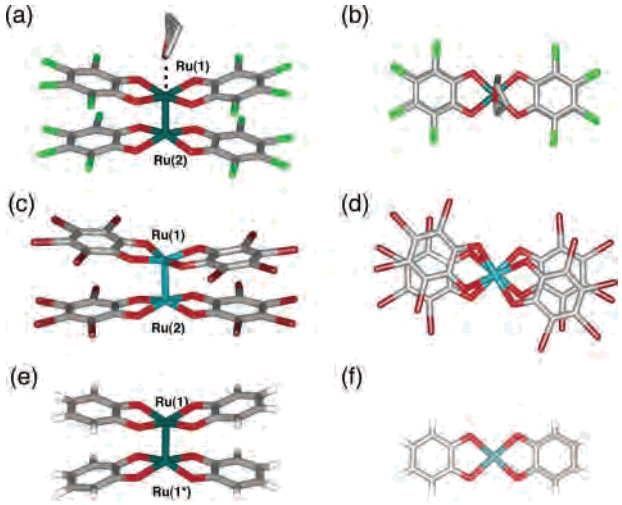

Figure 1. Representative trianionic unit in $[Na_3\{Ru_2(R_4Cat)_4\}]$ (R_4 = (a, b) $-Cl_4$ ($\mathbf{2_s}$), (c, d) $-Br_4$ ($\mathbf{3_s}$), and (e, f) $-H_4$ (**4**)). Hydrogen atoms of THFs, sodium cations, and cocrystallized solvent molecules are omitted for clarity. Color code: Ru, deep green; C, gray; O, red; H, white; Cl, light green; Br, brown.

octahedral or a five-coordinated square pyramidal geometry. In the former, the Ru atom is coordinated by an adjacent Ru atom, four O atoms from two coplanar dioxolene ligands, and an O atom from axial THF, while the latter has a vacant site in the axial position. The combination of the two coordination geometries leads to three different dinuclear core structures defined as **I**−**III**, respectively (Chart 2). The core structure **I** is found in $\mathbf{2'_s}$ and $\mathbf{3'_s}$ (vide infra), where two THF molecules coordinate to both axial sites of the $[Ru_2]$ cores (Figure 2a,c). On the other hand, $\mathbf{2_s}$ has the core structure **II**, which contains the six-coordinated and the five-coordinated Ru atom in an opposite way, giving an asymmetric dinuclear structure. Finally, complex $\mathbf{3_s}$ crystallized from acetone/hexane, **4**, and the complexes, **5′** and $\mathbf{6'_s}$, with 3,5(6)-di-*tert*-butyl substituted ligands (vide infra) are classified as the core structure **III**, where the two axial positions are vacant sites. The numbers of axial ligands are summarized in Table 2.

It is important to mention the oxidation state of the dioxolene ligands before further description of the molecular structures, since the dioxolene ligands have been known to show rich redox states including catecholate (Cat^{2-}), semiquinonate ($SQ^{\bullet-}$), and benzoquinone (BQ) with dianionic, monoanionic, and neutral states, respectively.[18] The assignment of each oxidation state has been conveniently made by X-ray crystal structural analysis on the basis of the well-known relationship between the C−O and C−C bond distances and the corresponding oxidation state.[19] For example, the C−O distance tends to change from 1.23 Å for BQ to longer values 1.29 and 1.34 Å for the $SQ^{\bullet-}$ and Cat^{2-} forms, respectively.[20] The bond distance is associated with the number of electrons occupying in the π^* orbital of BQ, which is principally localized at the C−O moiety.[21] All of the values observed for the present complexes fall in the range of 1.33−1.353 Å (Table 2), which convincingly indicates that the ligands are in the fully reduced, dianionic Cat^{2-} form. This indicates that no heterogeneous charge distribution occurs within the molecules, and therefore, no localized ligand-based mixed-valence character is recognized,[22] even in the asymmetric core structure **II**. According to these results, we have concluded that the ligation of the four R_4Cat^{2-} ligands to two Ru atoms commonly provides −8 formal anionic charges around the $[Ru_2]$ cores in $\mathbf{2_s}$, $\mathbf{3_s}$, and **4**. This consideration also leads to the formal oxidation number of each $[Ru_2]$ core based on the number of countercations. Since complexes $\mathbf{2_s}$, $\mathbf{3_s}$, and **4** possess three Na^+ cations/dimeric unit, the central $[Ru_2]$ core should have +5 formal positive charges, leading to a general formulation of $[Na_3\{Ru_2(R_4Cat)_4\}]$ with the $[Ru_2]^{5+}$ core. This conclusion therefore indicates that the four acetate ligands in $Ru_2(OAc)_4Cl$ were completely replaced by the R_4Cat^{2-} ligands, maintaining the oxidation state of the diruthenium $[Ru_2]^{5+}$ core.

The formation of the ligand-unsupported Ru−Ru bond is one of the most characteristic structural features of the $[Na_3\{Ru_2(R_4Cat)_4\}]$ complexes. The bond distances of $\mathbf{2_s}$, $\mathbf{3_s}$, and **4** are in the range 2.246(1)−2.273(1) Å, while the longest and the shortest distance is found in $\mathbf{2_s}$ and **4**, respectively. The observed Ru−Ru distances are equal to or shortened compared with the values for paddle-wheel type dinuclear complexes (ca. 2.248−2.431 Å)[1,23] and those for

(18) Pierpont, C. G. *Coord. Chem. Rev.* **2001**, *216*−*217*, 99.
(19) Pierpont, C. G.; Lange, C. W. *Prog. Inorg. Chem.* **1994**, *41*, 331.
(20) Boone, S. R.; Pierpont, C. G. *Polyhedron* **1990**, *9*, 2267.
(21) Wheeler, D. E.; Rodriguez, J. H.; McCusker, J. M. *J. Phys. Chem. A* **1999**, *103*, 4101.
(22) (a) Chang, H.-C.; Mochizuki, K.; Kitagawa, S. *Inorg. Chem.* **2002**, *41*, 4444. (b) Chang, H.-C.; Miyasaka, H.; Kitagawa, S. *Inorg. Chem.* **2001**, *40*, 146.

Chart 2. Classification of Core Structures Based on the Number of Axial Ligands

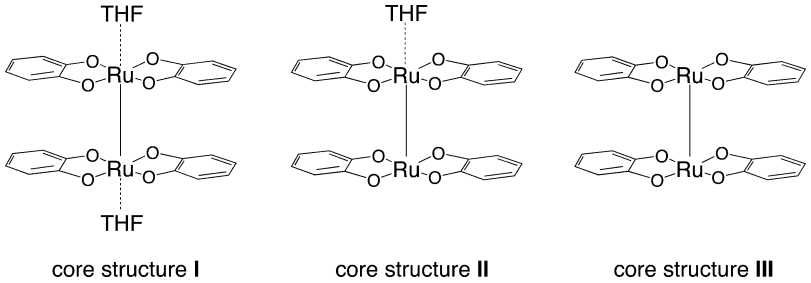

Chart 3. Definition of Deviation, *d*/Å, and Twist Angle, *θ*/deg

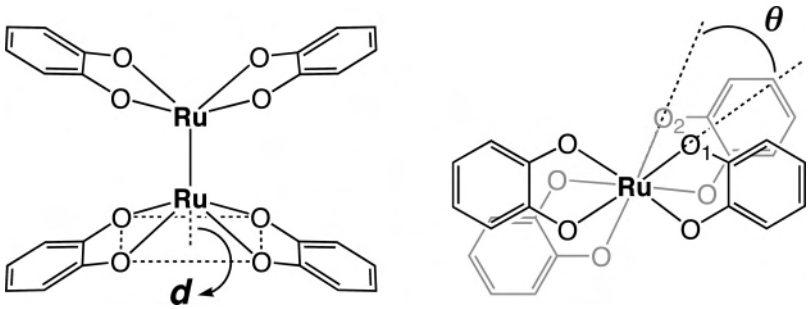

dinuclear Ru complexes with ligand-unsupported Ru−Ru bonds, 2.2782(4) and 2.293(2) Å for $[Ru_2(tmtaa)_2]BPh_4$ (tmtaa = dibenzotetramethyltetraaza[14]annulene)[24] and $[Ru_2(TPP)_2]PF_6$ (TPP = tetraphenylporphyrin),[25] respectively.

Two structural parameters concerning the structural deviations caused by the ligand-unsupported Ru−Ru bonds well describe the overall structures of the present complexes on the basis of the following experimental results. First, all of the complexes have a domed conformation with a displacement of the Ru atom from the plane of the four coordinating O_{Cat} atoms from two cofacial R_4Cat^{2-}. The deviation from the plane toward the Ru counterpart is defined as the *d* value depicted in Chart 3. The *d* values in $\mathbf{2_s}$, $\mathbf{3_s}$, and **4** range from 0.271(3) to 0.388(3) Å (Table 2), depending on the substituents on the catecholates. Among the observed values, the largest deviation observed for **4** is comparable to 0.379 Å observed for $[Ru_2(TPP)_2]PF_6$[25] but much smaller than 0.432 and 0.425 Å for $[Ru_2(tmtaa)_2]BPh_4$.[24] The deviations could be attributable to the intramolecular repulsive interactions between the six-membered aromatic ring, the substituents, and O_{Cat} atoms of the ligands[26] (also see subsection 3.5.2). It is noteworthy that, in the complexes with asymmetric core structure **II**, a smaller deviation is observed for the octahedral Ru atom. For example, the *d* value for Ru(1) of $\mathbf{2_s}$ is smaller than that for square pyramidal Ru(2) by ca. 0.1 Å. This is caused by presence of the steric hindrance between the THF and the R_4Cat^{2-} ligands (Figure 1), especially between their O atoms. The distortion of the Ru atom can also be reflected in the Ru−Ru−O_{Cat} angle for each complex, as listed in Table 2. The observed values are in the range of 97.7−101.2°, deviating from the 90° for ideal square pyramidal and/or octahedral coordination geometry.

For the second parameter, we can point out a rotational freedom of the dinuclear complexes along the Ru−Ru bonding axis. The deviation from the ideal eclipsed form can be measured by a twist angle, *θ*, which is defined by the dihedral angle between $O_1-Ru_1-Ru_2-O_2$, as shown in Chart 3. Complexes $\mathbf{2_s}$ and **4** show an almost eclipsed form with *θ* values close to 0° (Table 2), while a staggered form with *θ* less than 20° is found in $\mathbf{3_s}$. Obviously, the complexes have two additional degrees of freedom, *d* and *θ*, in their molecular structures based on the ligand-unsupported Ru−Ru bonds (also see subsection 3.5.2).

3.3. Syntheses and Structures of the One-Electron-Oxidized Family, $[Na_2\{Ru_2(R_4Cat)_4\}]$. Chemical oxidation of the $[Na_3\{Ru_2(R_4Cat)_4\}]$ (**1**−**4**) family by Ag(I) salt causes a slight color change of the solution, and the corresponding one-electron-oxidized complex was isolated by recrystallization (eq 2 and route A in Scheme 1). The single-crystal analysis of $\mathbf{2'_s}$[6] and $\mathbf{3'_s}$ and the elemental analysis data showed that each complex commonly includes two Na^+ cations/$[Ru_2]$ unit, affording a family of general formulation of $[Na_2\{Ru_2(R_4Cat)_4\}]$ (**1′**−**4′**).

$$[Na_3\{Ru_2(R_4Cat)_4\}]\ (\mathbf{1}-\mathbf{4}) + AgOCOCF_3 \rightarrow [Na_2\{Ru_2(R_4Cat)_4\}]\ (\mathbf{1'}-\mathbf{4'}) + NaOCOCF_3 + Ag \quad (2)$$

Although the stoichiometric amount of silver salt was required for isolation of **1′**−**4′**, complexes **5′** and **6′** having the same stoichiometry as **1**−**4** were isolated directly from the mixture of $Ru_2(OAc)_4Cl$ and 3,5(6)-DTBCatH_2 in the absence of the silver salts (route B in Scheme 1). Even under extremely strict control for air and/or excess water contamination, an in situ one-electron oxidation might exceptionally occur during the reaction, directly providing the one-electron-oxidized species. The low oxidation potential of

(23) Bear, J. L.; Han, B.; Huang, S.; Kadish, K. M. *Inorg. Chem.* **1996**, *35*, 3012.
(24) Hesschenbrouck, J.; Solari, E.; Scopelliti, R.; Floriani, C.; Re, N. *J. Organomet. Chem.* **2000**, *596*, 77.
(25) Collman, J. P.; Harford, S. T. *Inorg. Chem.* **1998**, *37*, 4152.
(26) Mota, F.; Novoa, J. J.; Losada, J.; Alvarez, S.; Hoffmann, R.; Silvestre, J. *J. Am. Chem. Soc.* **1993**, *115*, 6216.

Table 3. Redox Potentials (V vs Fc/Fc^+) of $[Na_n\{Ru_2(R_4Cat)_4\}]$ (n = 3 or 2) with $[Ru_2]^{5+}/[Ru_2]^{6+}$ Cores

			redox potentials/V (ΔE_{pp}/V)			
	R_4	rest potential/V			$[Ru_2]^{6+}/[Ru_2]^{5+}$	$[Ru_2]^{5+}/[Ru_2]^{4+}$
1[a]	$-F_4$	−1.22		0.52[c]	−0.74 (0.26)	−1.71 (0.18)
2[a]	$-Cl_4$	−0.82		0.50[c]	−0.55 (0.10)	−1.65 (0.14)
3[a]	$-Br_4$	−0.81		0.45[c]	−0.53 (0.10)	−1.61 (0.10)
4[b]	$-H_4$	−1.66		−0.26[c]	−1.36 (0.12)	−2.09[d]
1′[a]	$-F_4$	−0.46		0.41[c]	−0.80 (0.35)	−1.85 (0.46)
2′[a]	$-Cl_4$	−0.42		0.41[c]	−0.60 (0.11)	−1.71 (0.13)
3′[a]	$-Br_4$	−0.42		0.36[c]	−0.62 (0.12)	−1.70 (0.11)
4′[b]	$-H_4$	−0.99		−0.26[c]	−1.37 (0.16)	−2.10[d]
5′[a]	−3,5-DTB	−0.59		−0.33[c]	−1.41 (0.21)	
6′[a]	−3,6-DTB	−0.99	−0.35 (0.11)	−0.74 (0.09)	−1.46 (0.27)	

[a] THF solution containing 2 mM of complex and 0.2 M n-Bu_4NPF_6, 10 mV/s. [b] DMF solution containing 2 mM of complex and 0.2 M n-Bu_4NPF_6, 10 mV/s. [c] E_{ap}. [d] E_{cp}.

$[Ru_2^{II,III}(3,5(6)\text{-DTBCat})_4]^{3-}$, compared with those of **1**−**4** (vide infra; Table 3), would be responsible for the in situ oxidation. The reduction of the $[Ru^{II}Ru^{III}(OAc)_4]^+$ cation to the one-electron reduced $[Ru^{II}_2(OAc)_4]$ by $[Ru^{II}Ru^{III}(3,5(6)\text{-DTBCat})_4]^{3-}$ could occur as one of the plausible reaction as shown in eq 3. The reduced $[Ru^{II}_2(OAc)_4]$ species will also participate in the following ligand substitution reaction with $3,5(6)\text{-DTBCat}^{2-}$, affording $[Ru^{III}_2(3,5(6)\text{-DTBCat})_4]^{2-}$ accompanying the in situ redox reaction. Therefore, the use of starting materials having low reduction potentials may be necessary to stabilize the $[Ru^{II}Ru^{III}(3,5(6)\text{-DTBCat})_4]^{3-}$ species.

$$[Ru^{II}Ru^{III}(OAc)_4]^+ + [Ru^{II}Ru^{III}(3,5(6)\text{-DTBCat})_4]^{3-} \rightleftarrows [Ru^{II}_2(OAc)_4] + [Ru^{III}_2(3,5(6)\text{-DTBCat})_4]^{2-} \quad (3)$$

Representative structures of the dianionic unit in $[Na_2\{Ru_2(R_4Cat)_4\}]$ (**2′**$_s$, **3′**$_s$, **5′**, and **6′**$_s$) are drawn in Figure 2, and the crystallographic data and structural parameters are listed in Tables 1 and 2. The coordination geometry around each Ru atom is either the symmetric core structure **I** or **III**, affording the same geometry, Oh or Sp, for the two Ru atoms in each complex. The $C-O_{Cat}$ bond distances of the complexes fall in the range of 1.353−1.37 Å, implying the retention of the Cat^{2-} form after the one-electron oxidation. The observation of the Cat^{2-} form in both $[Na_3\{Ru_2(R_4Cat)_4\}]$ and $[Na_2\{Ru_2(R_4Cat)_4\}]$ families indicates that the electron was removed from a metal-centered molecular orbital, leading to the increase of positive charge on the $[Ru_2]$ core during the oxidation process from $[Ru_2]^{5+}$ to $[Ru_2]^{6+}$. Thus, one could expect that the metal-centered oxidation would lead to significant structural changes around the central $[Ru_2]$ core.

3.4. Effects of Oxidation States on the Electronic Structures of the Diruthenium Complexes. 3.4.1. Structural Comparison between Two Redox Isomers with $[Ru_2]^{5+}$ and $[Ru_2]^{6+}$ Cores. It is known that the structural comparison of two different redox species provides important information about the electronic structure of each redox isomer.[24,27] Herein, we could also compare the structural parameters of the $[Na_3\{Ru_2(R_4Cat)_4\}]$ family with those of the one-electron-oxidized $[Na_2\{Ru_2(R_4Cat)_4\}]$ family. A clear structural difference between the two families is found for the central $[Ru_2]$ cores. First, the one-electron oxidation of the $[Na_3\{Ru_2(R_4Cat)_4\}]$ family causes a decrease in the $Ru-O_{Cat}$ bond distances by ca. 0.03 Å, as listed in Table 2, reflecting the increase of positive charge on the $[Ru_2]$ core upon oxidation. In addition, the Ru−Ru bond distances of the $[Na_2\{Ru_2(R_4Cat)_4\}]$ family are in the range 2.140(2)−2.2233(6) Å, which are apparently shorter than 2.246(1)−2.273(1) Å for the $[Na_3\{Ru_2(R_4Cat)_4\}]$ family by 0.05−0.10 Å. On the other hand, the $C-O_{Cat}$ bond distances of both families show characteristics of the Cat^{2-} form. These results strongly indicate that the oxidation of the $[Na_3\{Ru_2(R_4Cat)_4\}]$ family commonly occurs on the central $[Ru_2]^{5+}$ core rather than the ligand moieties to afford a $[Ru_2]^{6+}$ core.

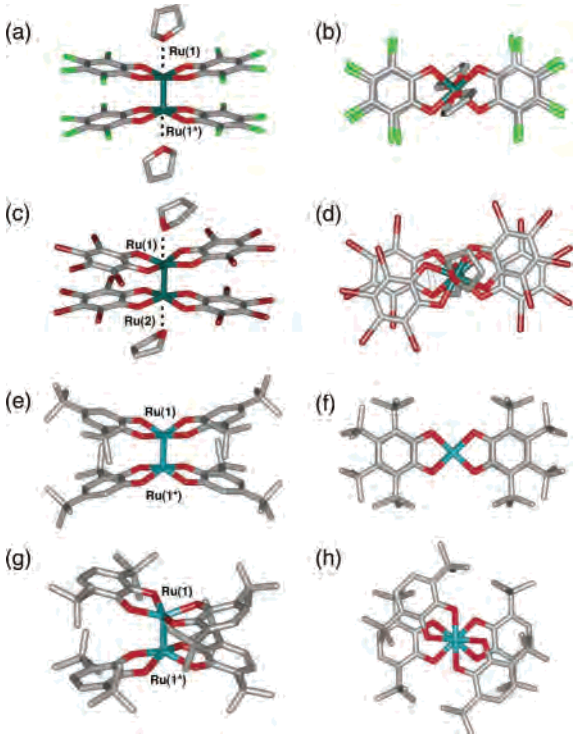

Figure 2. Representative dianionic unit in $[Na_2\{Ru_2(R_4Cat)_4\}]$ (R_4 = (a, b) $-Cl_4$ (**2′**$_s$), (c, d) $-Br_4$ (**3′**$_s$), (e, f) −3,5-DTB (**5′**), and (g, h) −3,6-DTB (**6′**$_s$)). Hydrogen atoms, sodium cations, and cocrystallized solvent molecules are omitted for clarity. Color code: Ru, deep green; C, gray; O, red; Cl, light green; Br, brown.

(27) (a) Cotton, F. A.; Yokochi, A. *Inorg. Chem.* **1997**, *36*, 567. (b) Tait, C. D.; Garner, J. M.; Collman, J. P.; Sattelberger, A. P.; Woodruff, W. H. *J. Am. Chem. Soc.* **1989**, *111*, 7806. (c) Cotton, F. A.; Yokochi, A. *Polyhedron* **1998**, *17*, 959.

The Ru−Ru bond distances of the two redox isomeric counterparts provide very useful information for the nature of frontier orbitals. The experimental data show the decrease in the Ru−Ru bond distances by ca. 0.05 Å in the $[Na_2\{Ru_2(X_4Cat)_4\}]$ (X = halogen atom) family compared with the $[Na_3\{Ru_2(X_4Cat)_4\}]$ family. This is virtually similar to that for the $[Ru_2^{5+/6+}(OEP)_2]$ (H_2OEP = 2,3,7,8,12,13,-17,18-octaethylporphyrin) couple[27b,28] and other paddle-wheel type diruthenium complexes having π^* frontier electrons,[29] indicating that one electron is removed from a metal-centered *antibonding* orbital during the chemical oxidation. For paddle-wheel type diruthenium complexes with O-donating ligands such as carboxylate, the electronic configuration has been shown to be $\sigma^2\pi^4\delta^2(\delta^*\pi^*)^3$ (bond order = 2.5) and $\sigma^2\pi^4\delta^2(\delta^*\pi^*)^2$ (bond order = 3) for the $[Ru_2]^{5+}$ and $[Ru_2]^{6+}$ cores, respectively, where the δ^* and π^* orbitals are accidentally degenerate as a result of orbital interaction between metal-centered δ^* and ligand-centered π orbitals.[30] In contrast, those for diruthenium complexes with ligand-unsupported Ru−Ru bonds have been assigned to be $\sigma^2\pi^4\delta^2\delta^{*2}\pi^{*1}$ (bond order = 2.5) and $\sigma^2\pi^4\delta^2\delta^{*2}$ (bond order = 3) for the complexes with $[Ru_2]^{5+}$[4,24,25] and $[Ru_2]^{6+}$ cores,[4,31,32] respectively, where the energy levels of δ^* and π^* orbitals are not degenerate.

To confirm the hypothetical electronic configurations in the present complexes, the magnetic susceptibility was measured for both families. If the $[Na_3\{Ru_2(R_4Cat)_4\}]$ (11 d electrons) and $[Na_2\{Ru_2(R_4Cat)_4\}]$ (10 d electrons) families had the electronic configurations of $\sigma^2\pi^4\delta^2\delta^{*2}\pi^{*1}$ and $\sigma^2\pi^4\delta^2\delta^{*2}$, respectively, the spin states of $S = 1/2$ and $S = 0$ could be expected. All of the $[Na_3\{Ru_2(R_4Cat)_4\}]$ (R_4 = $-F_4$, $-Cl_4$, $-Br_4$, and $-H_4$) family shows paramagnetic behavior with magnetic moments of 1.59−1.67 μ_B at 300 K (see Supporting Information). These values are comparable to the theoretical value, 1.73 μ_B, calculated for the $S = 1/2$ spin state ($g = 2.00$). In addition, the $[Na_3\{Ru_2(R_4Cat)_4\}]$ family shows an EPR signal with three components at g-values of $g_1 = 1.50$, $g_2 = 1.73$, and $g_3 = 2.13$ for **1**, $g_1 = 1.53$, $g_2 = 1.82$, and $g_3 = 2.19$ for **2**, and $g_1 = 1.56$, $g_2 = 1.86$, and $g_3 = 2.21$ for **3** in the frozen THF glasses at 77 K and $g_1 = 1.79$, $g_2 = 1.93$, and $g_3 = 2.01$ for **4** in the frozen DMF glass at the same temperature (see Supporting Information). All of these results therefore are consistent with the absence of degenerate frontier orbitals in the electronic configuration $\sigma^2\pi^4\delta^2\delta^{*2}\pi^*$ (bond order = 2.5) for $[Na_3\{Ru_2(R_4Cat)_4\}]$. On the other hand, the $[Na_2\{Ru_2(R_4Cat)_4\}]$ family demonstrates diamagnetic behavior and normal NMR signals for the $[Na_2\{Ru_2(3,5(6)\text{-}DTBCat)_4\}]$ complexes, supporting the electronic configuration of $\sigma^2\pi^4\delta^2\delta^{*2}$ with the bond order of 3.

3.4.2. Electrochemical Behavior of the Redox Isomers. To ensure the assignment for the one-electron oxidation process together with the intramolecular charge distribution derived from the structural characterization, we now compare the electrochemical data for **1**/**1′**, **2**/**2′**, **3**/**3′**, and **4**/**4′** couples investigated by cyclic voltammetry (CV) in either THF (**1**/**1′**, **2**/**2′**, **3**/**3′**) or DMF (**4**/ **4′**) solution. Figures 3 and 4a demonstrate the voltammograms of the complexes with $[Ru_2]^{5+}$ and $[Ru_2]^{6+}$ cores, and the redox potentials for each complex are summarized in Table 3. Complexes **1**−**3** studied in THF solutions have rest potentials at −1.22 (**1**), −0.82 (**2**), and −0.81 V (**3**), respectively. The complexes undergo one quasi-reversible one-electron reduction process near −1.7 V in the negative scan, while one quasi-reversible one-electron oxidation and one irreversible one-electron oxidation process were found near −0.6 and 0.5 V, respectively, for the positive scan. On the other hand, the rest potentials for the oxidized species (Figure 3), **1′**−**3′**, were shifted positively, but the overall features of the voltammograms are essentially identical with those of **1**−**3**. In addition, the irreversible oxidation waves were commonly found near 0.4 V. The similar redox waves are observed for the voltam-

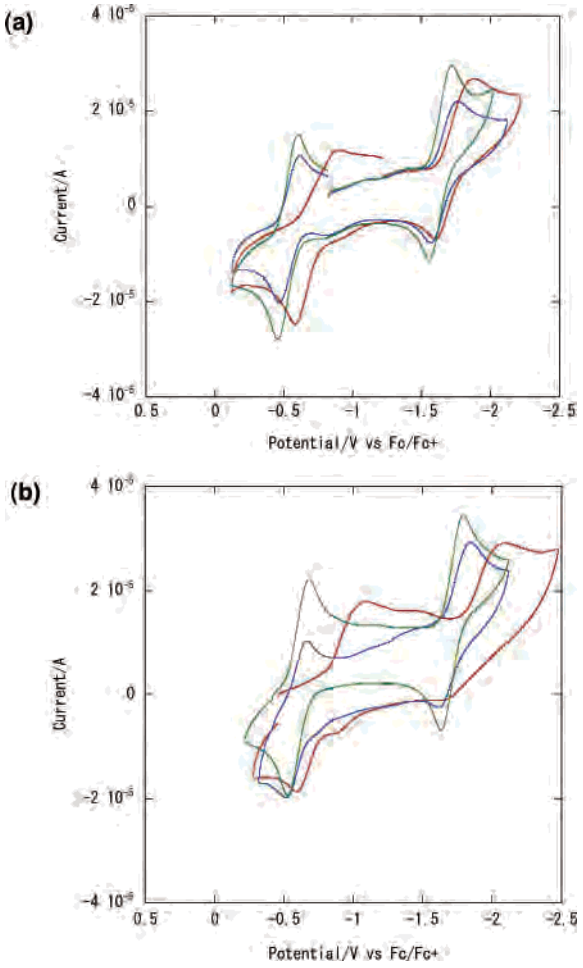

Figure 3. Cyclic voltammograms of (a) $[Na_3\{Ru_2(X_4Cat)_4\}]$ (X = −F (**1**, red line), −Cl (**2**, blue line), and −Br (**3**, green line)) and (b) $[Na_2\{Ru_2(X_4Cat)_4\}]$ (X = −F (**1′**, red line), −Cl (**2′**, blue line), and −Br (**3′**, green line)). Conditions: 2 mM THF solution containing 0.2 M n-Bu_4NPF_6; 100 mV/s; room temperature; N_2.

(28) Asahina, H.; Zisk, M. B.; Hedman, B.; McDevitt, J. T.; Collman, J. P.; Hodgson, K. O. *J. Chem. Soc., Chem. Commun.* **1989**, 1360.
(29) Ebihara, M.; Nagaya, N.; Kawashima, N.; Kawamura, T. *Inorg. Chim. Acta* **2003**, *351*, 305.
(30) Norman, J. G.; Renzoni, G. E.; Case, D. A. *J. Am. Chem. Soc.* **1979**, *101*, 5256.
(31) Jérôme, F.; Billier, B.; Barbe, J.-M.; Espinoza, E.; Dahaoui, S.; Lecomte, C.; Guilard, R. *Angew. Chem., Int. Ed.* **2000**, *39*, 4051.
(32) Simkhovich, L.; Luobeznova, I.; Goldberg, I.; Gross, Z. *Chem.—Eur. J.* **2003**, *9*, 201.

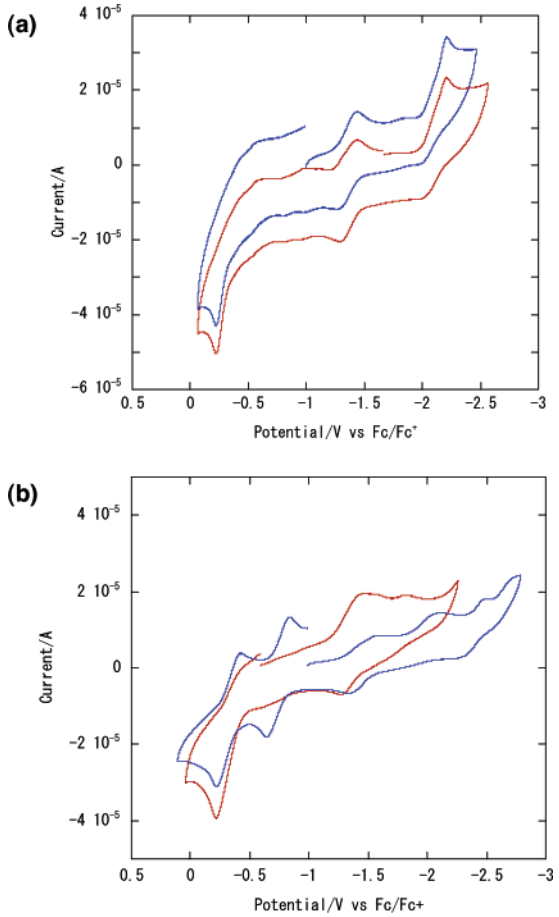

Figure 4. Cyclic voltammograms of (a) $[Na_3\{Ru_2(H_4Cat)_4\}]$ (**4**, red line) and $[Na_2\{Ru_2(H_4Cat)_4\}]$ (**4′**, blue line) in DMF and (b) $[Na_2\{Ru_2(3,5\text{-}DTBCat)_4\}]$ (**5′**, red line) and $[Na_2\{Ru_2(3,6\text{-}DTBCat)_4\}]$ (**6′**, blue line) in THF. Conditions: 2 mM solution containing 0.2 M n-Bu_4NPF_6; 100 mV/s; room temperature; N_2.

mograms of **4** and **4′** measured in DMF solutions (see subsection 3.5.4). The similarity in the voltammograms of two redox counterparts indicate that the dimeric structures are retained after the one-electron oxidation, and the one-electron chemical oxidation of **1**−**4** by the silver(I) salts can be attributed to the oxidation of the $[Ru_2]$ core rather than the ligand moieties, as shown in eq 4. All of the structural changes found for the two redox counterparts listed in Table 2 are consistent with this consideration.

$$[Ru^{II}Ru^{III}(R_4Cat)_4]^{3-}\ (\mathbf{1}-\mathbf{4}) \rightleftarrows [Ru^{III}{}_2(R_4Cat)_4]^{2-}\ (\mathbf{1'}-\mathbf{4'}) + e^- \quad (4)$$

The couples observed in the region of −1.6 to −1.7 V in both families could be attributable to the metal-centered reduction, because there is no chance to accept the electron on the ligand moieties due to the fully reduced nature of the R_4Cat^{2-} ligands. Therefore, we assigned these redox couples to the reduction of the $[Ru_2]$ core from $[Ru_2]^{5+}$ to $[Ru_2]^{4+}$ as shown in eq 5. As a whole, three different diruthenium species, $[Ru_2(R_4Cat)_4]^{4-}$, $[Ru_2(R_4Cat)_4]^{3-}$, and $[Ru_2(R_4Cat)_4]^{2-}$, can exist in solution, and these are electrochemically converted to each other through the metal-centered redox process.

$$[Ru^{II}Ru^{III}(R_4Cat)_4]^{3-}\ (\mathbf{1}-\mathbf{4}) + e^- \rightleftarrows [Ru^{II}{}_2(R_4Cat)_4]^{4-} \quad (5)$$

3.5. Substituent-Induced Structural and Physicochemical Changes. Another important aspect of the complexes is the substituent effects of the R_4Cat^{2-} ligands on the structural and physicochemical properties of the diruthenium complexes. In the case of paddle-wheel type dinuclear complexes, the structural and electronic modulations have been independently investigated by several research groups.[7] In contrast, very little attention has been paid to systematic examination of their effects on the ligand-unsupported M−M bonds. One can, however, easily imagine that the ligand-unsupported M−M bonded structures have a greater potential to vary their molecular and electronic structures by substituent groups on the basis of their structural flexibilities. This background prompted us to synthesize a series of diruthenium complexes by using the six different catecholate derivatives shown in Chart 1. The molecular structures of diruthenium complexes with four and six different kinds of substituents for the $[Na_3\{Ru_2(R_4Cat)_4\}]$ and $[Na_2\{Ru_2(R_4Cat)_4\}]$ families, respectively, were isolated, and most of them were structurally characterized. The substituent effects, in general, include steric and electronic contributions to the molecular and electronic structures of the molecules. Therefore, it is often difficult to independently extract these two separate contributions. However, the systematic isolation and crystallographic analysis show that the six different substituted groups on R_4Cat^{2-} can modulate four fundamental structural parameters of the dimeric structures: (1) Ru−Ru bond distances; (2) rotational angle, θ; (3) deviation, d; (4) axial ligation. Complicated correlations between these parameters were recognized; i.e., one cannot independently control one of them by changing substituents. However, by examination of apparent tendencies, these parameters could be partially interpreted in terms of the substituent effects.

3.5.1. Substituent Effects on Ru−Ru Bond Distances. The Ru−Ru bond distances are significantly changed by the varying substituents of the R_4Cat^{2-} ligands, as demonstrated in Table 2. Interestingly, the Ru−Ru bond distances in both $[Na_3\{Ru_2(R_4Cat)_4\}]$ and $[Na_2\{Ru_2(R_4Cat)_4\}]$ families are shortened as the electron-donating nature of the substituents increases. The observed Ru−Ru bond distances are a balance between the shortening effect of the removed electrons from the antibonding orbitals and the elongation effect of the repulsive interaction between two positively charged Ru atoms.[27a] The electronic effects of the substituents could significantly contribute to the variations of the Ru−Ru bond distances, because these lead to predictable energetic perturbations in the σ- and π-orbital energies of the substituted catecholates. First, the σ-donating ability of R_4Cat^{2-} is expected to decrease in the order of calculated pK_a: −3,6-DTB (14.33) > −3,5-DTB (14.14) > $-H_4$ (12.84) > $-F_4$ (9.63) > $-Cl_4$ (9.02) > $-Br_4$ (8.84).[33] Because the negative charges reside primarily on the O_{Cat} atoms of R_4Cat^{2-}, the electron-donating substituents can reduce the positive charge

(33) The pK_a values were calculated by the ACD pK_a DB software package of Advanced Chemistry Development Inc.

on the [Ru_2] core by relatively high electron density on the O_{Cat} atoms, giving a shorter Ru−Ru bond, while the electron-withdrawing substituents induce a buildup of positive charge on the [Ru_2] core, giving a longer Ru−Ru bond. Second, the orbital interactions between the R_4Cat^{2-} and [Ru_2] core can appear also between dπ orbitals from the [Ru_2] core and the pπ orbital of the R_4Cat^{2-}. To obtain a deeper understanding of these interactions, accurate molecular orbital calculations need to be carried out. Finally, we recognized the effect of the axial ligands on the Ru−Ru bond distances, as shown in the section 3.5.3.

3.5.2. Substituent Effects on the θ and *d* Values. We found that the variations in the rotational angles around the Ru−Ru bond can be regarded as the result of the substituent effects. Complex **4** with $-H_4$ substituents and $\mathbf{2}_s$ and $\mathbf{2'}_s$ with $-Cl_4$ show a perfect eclipsed form or weakly staggered form with small θ values. The eclipsed form was also found for **5′**, where the presence of two −*t*-Bu substituents on the 3- and 5-positions forces the complex into an eclipsed form with the small θ value of 1.4°. In this complex, only the eclipsed form can effectively avoid the intramolecular repulsive interactions between the −DTB substituents. On the other hand, complexes $\mathbf{3}_s$ and $\mathbf{3'}_s$ show the θ value of approximately 20° deviating from the eclipsed form, and complex $\mathbf{6'}_s$ also shows a higher degree of rotation with the largest θ value of 50.8°. Steric hindrances could appear between the Br atoms in $\mathbf{3}_s$ and $\mathbf{3'}_s$ and the −*t*-Bu substituents in $\mathbf{6'}_s$. It seems likely that the observed angles are the best compromises that can stabilize the molecular structure with the minimum intramolecular instability caused by the repulsion between the substituents. Comparison of the observed *d* and θ values makes us find the primary tendency in structural deviation for reducing intramolecular steric hindrances. The complexes with relatively small substituents (−H and −Cl) increase the *d* values (*d*-mechanism) so that the substituents apart far from each other. On the other hand, the θ values are regulated (θ-mechanism) to reduce the intramolecular steric hindrances in the cases of complexes with relatively bulky substituents (−Br and −3,5-DTB) in addition to the *d*-mechanism.[34] Both deviations, in general, tend to be increasing, when the Ru−Ru bond distance becomes shorter because of the expected increases of repulsive interactions between the aromatic rings, the substituents, and O_{Cat} atoms. Finally, both mechanisms could simultaneously contribute to the molecular structures of $\mathbf{6'}_s$ because of the larger spatial size of the −*t*-Bu substituents and the relatively short Ru−Ru bond.

3.5.3. Substituent Effects on Axial Ligation. Our systematic studies demonstrate that the number of axial ligands tends to decrease as the electron-donating nature of the substituents increases. The effects of axial ligation on paddle-wheel type dinuclear complexes[23,35] showed that σ-donating interactions and/or π-acceptability of the axial ligand increase the σ orbital energy, both causing elongation of the Ru−Ru bond distances.[35a] Therefore, observed trends in the variation of Ru−Ru bond distances results, in part, from the axial ligation effects. The steric hindrance coming from six different substituents of the equatorial ligation is the first factor that governs the axial ligations. This effect can be recognized from the absence of the axial ligand in the complexes with −DTB substituents with an extremely short Ru−Ru bond and large distortion, *d*, more than 0.4 Å, which is larger than those of a series of complexes with X_4Cat^{2-} ligands ($d \sim 0.3$ Å). Second, the electronic effect of the substituents through the equatorial chelation might be the reason for the observed trends in the axial ligation. Because the ability to accept the lone pair from THFs strongly depends on the localized positive charges on the Ru atoms, the σ-donating ability of the substituents must be considered when interpreting the axial ligations.

3.5.4. Substituent Effect on Electrochemical Properties. The cyclic voltammograms observed for the [Na_3{Ru_2-($R_4Cat)_4$}] and [Na_2{$Ru_2(R_4Cat)_4$}] families are given in Figures 3 and 4, and the redox potentials are summarized in Table 3. Among the [Na_3{$Ru_2(R_4Cat)_4$}] family, the series of [Na_3{$Ru_2(X_4Cat)_4$}] commonly undergo one electrochemically quasi-reversible one-electron oxidation and reduction process around −0.6 and −1.7 V, respectively (Figure 3a). As shown above, the one-electron-oxidized family, [Na_2{$Ru_2(X_4Cat)_4$}], demonstrates voltammograms quite similar to those of the [Na_3{$Ru_2(X_4Cat)_4$}] family as given in eqs 4 and 5. Another couple of **4**/**4′** with $-H_4$ substituents demonstrates quite similarly two redox couples near −1.4 and −2.1 V (Figure 4a), which could be assigned to a metal-centered two-step one-electron redox process (eqs 4 and 5). A common feature of these series is the appearance of three different diruthenium species, $[Ru_2(R_4Cat)_4]^{2-}$, $[Ru_2(R_4Cat)_4]^{3-}$, and $[Ru_2(R_4Cat)_4]^{4-}$, and these can be interconverted electrochemically without destroying the Ru−Ru bond (eq 6).

$$[Ru_2(R_4Cat)_4]^{2-}\ (\mathbf{1'}-\mathbf{4'}) \rightleftarrows [Ru_2(R_4Cat)_4]^{3-}\ (\mathbf{1}-\mathbf{4}) \rightleftarrows [Ru_2(R_4Cat)_4]^{4-} \quad (6)$$

The feature of the voltammogram was drastically changed when the complex possesses −DTB substituents. The rest potential of **5′** was found at −0.59 V, and its cyclic voltammogram (Figure 4) consists of one quasi-reversible reduction couple at −1.41 V and an irreversible anode peak at −0.33 V, which appears in the positive scan. The rest potential of the complex is shifted negatively about 0.17 V relative to that of **2′**. This indicates that complex **5′** is more easily oxidized and concurrently more difficult to reduce to the $[Ru_2(3,5\text{-DTBCat})_4]^{3-}$ species than the corresponding process for the series of [Na_2{$Ru_2(X_4Cat)_4$}] (eq 6). These trends are attributable to the strong substituent effects due to the electron-donating nature of the −DTB substituents. In fact, the first reduction peak of **5′** was moved to −1.41 V, which shifts ca. −0.81 V compared with that of **2′**. The further redox couple attributed to reduction to the [Ru_2(3,5-

(34) The axial coordination of THF contributes as second factor in the *d* as shown in section 3.2. It suppresses the increase of the *d* value.

(35) (a) Chisholm, M. H.; Christou, G.; Folting, K.; Huffman, J. C.; James, C. A.; Samuels, J. A.; Wesemann, J. L.; Woodruff, W. H. *Inorg. Chem.* **1996**, *35*, 3643. (b) Xu, G.; Campana, C.; Ren, T. *Inorg. Chem.* **2002**, *41*, 3521. (c) Vamvounis, G.; Caplan, J. F.; Cameron, T. S.; Robertson, K. N.; Aquino, M. A. S. *Inorg. Chim. Acta* **2000**, *304*, 87.

$DTBCat)_4]^{4-}$ species could not be observed in **5′** up to the negative end of the potential window.

$$\text{oxidized species} \leftarrow [Ru_2(3,5\text{-DTBCat})_4]^{2-}\ (\mathbf{5'}) \rightleftarrows [Ru_2(3,5\text{-DTBCat})_4]^{3-} \quad (7)$$

Surprisingly, the voltammogram of **6′** is clearly dissimilar from either those of **1′**−**4′** or **5′**. Complex **6′** shows a rest potential at −0.99 V, which is shifted ca. −0.57 and −0.40 V compared with those of **2′** and **5′**, respectively. The complex has one redox couple at −1.46 V attributable to the reduction of $[Ru_2]^{6+}$ to $[Ru_2]^{5+}$,[36] indicative of the highest electron-donating ability, in addition to two well-defined quasi-reversible one-electron oxidations are found at −0.74 and −0.35 V for the positive scan. The low reduction potential indicates a much stronger electron-donating effect of the −*t*-Bu substituted at the 3- and 6-positions of the catecholate compared with 3,5-$DTBCat^{2-}$. Furthermore, the exceptional ability of the 3,6-DTB substituents can be recognized by the unexpected observation of the stepwise two oxidations. These redox couples could be assigned to either a metal-centered oxidation, giving species with the $[Ru_2]^{7+}$ and the $[Ru_2]^{8+}$ core, or a ligand-centered oxidation, formally generating the $SQ^{\bullet-}$ radical ligand (eq 8). Efforts are being made to isolate and characterize the oxidation products of **6′**.[37] In both families of $[Na_n\{Ru_2(R_4Cat)_4\}]$ (n = 2 or 3), the redox potentials also followed the same trend of calculated pK_a. Interestingly, the redox potentials of the complexes are affected not only by the substituents as shown in this section but also by the cations bound to the complexes.[11]

$$\text{L/M-centered second oxidation} \rightleftarrows \text{L/M-centered first oxidation} \rightleftarrows [Ru_2(3,6\text{-DTBCat})_4]^{2-}\ (\mathbf{6'}) \rightleftarrows [Ru_2(3,6\text{-DTBCat})_4]^{3-} \quad (8)$$

4. Conclusion

In this manuscript, we have comprehensively examined the factors affecting the structural, electrochemical, and spectrochemical properties of the diruthenium complexes with ligand-unsupported Ru−Ru bonds containing catecholate derivatives. The results in the manuscript can be summarized as follows from several perspectives. (1) Synthesis of the diruthenium complexes with ligand-unsupported Ru−Ru bonds was carried out and diversified by the use of six different substituent groups. The synthetic methodology summarized in Scheme 1 allows us to control the oxidation states of the complexes with varying substituents on R_4Cat^{2-}. The conversion of the ligand-supported M−M bonds to the unsupported M−M bonds was proven to be useful for isolating direct M−M-bonded systems. This synthetic methodology can be generalized in the synthesis of M−M-bonded compounds with highly negatively charged chelating ligands. (2) We have demonstrated how the oxidation state of the complexes affects the structures and physicochemical properties of the complexes. Two redox counterparts of the diruthenium complexes with $[Ru_2]^{5+}$ and $[Ru_2]^{6+}$ cores with electron configuration of $\sigma^2\pi^4\delta^2\delta^{*2}\pi^*$ and $\sigma^2\pi^4\delta^2\delta^{*2}$, respectively, were structurally and electrochemically correlated. (3) The substituent effects on the diruthenium complexes with ligand-unsupported Ru−Ru bonds were revealed for the first time both in the solid state and in solution. In the solid state, the substituents significantly affect the structural parameters such as θ, d, and the Ru−Ru bond distances. In addition, those effects were clearly observed in the redox potential of the complexes. The redox activity of the R_4Cat^{2-} ligand could be an additional redox-tunable center, providing a useful method to control the electronic structure of the bimetallic cores with ligand-unsupported M−M bonds. From this point of view, the presence of two electrochemical couples in $[Ru_2(3,6\text{-DTBCat})_4]^{2-}$ would allow the generation of the isolable oxidation products that give us an opportunity to investigate further oxidation species. The results in this manuscript illustrate successive strategies of controlling the characteristic structures and properties of ligand-unsupported M−M systems and open a new route to design multifunctional M−M-bonded complexes.

Acknowledgment. We thank Prof. Takashi Kawamura for assistance with the EPR measurements and for discussion, and we acknowledge financial support by a Grant-in-Aid for Scientific Research from The Ministry of Education, Culture, Sports, Science, and Technology of Japan.

Supporting Information Available: Synthetic procedures of all the complexes, descriptions of individual crystal structures, temperature-dependent magnetic susceptibility of **1**−**4**, EPR spectra of **1**−**4**, figures of isomers for $[Ru_2(3,5\text{-DTBCat})_4]^{2-}$, the ^{1}H NMR spectrum of **5′**, absorption spectra of **1**−**4** and **1′**−**6′** (PDF), and X-ray crystallographic data for **3**$_s$, **4**, **3′**$_s$, **5′**, and **6′**$_s$ in CIF format. This material is available free of charge via the Internet at http://pubs.acs.org.

IC048251M

(36) The original voltammogram shows time dependency. Standing the solution leads to a gradual growth the peaks around −1.9 and −2.4 V. The cation exchange of Na^+ to *n*-Bu_4N^+, which comes from the electrolyte *n*-Bu_4NPF_6, is the most plausible reason for the observed time dependence.[11]

(37) The observed differences in the electrochemical properties of **5′** and **6′** cannot be clearly interpreted at this stage, but the dissimilarity of the rotational configurations would be one of the main reasons. As demonstrated in Figure 2, complex **5′** shows a perfect eclipsed form, while complex **6′**$_s$ has a staggered form with the θ values of 50.8°. Probably, the observed differences in the electrochemical properties come from the different internal structural instability caused by the repulsion between the O_{Cat} atoms in each oxidized species with the eclipsed and staggered forms for the one-electron oxidized species of **5′** and **6′**, respectively.